COBEM 2021 26th International Congress of Mechanical Engineering
ABCM Associação Brasileira de Engenharia e Ciências Mecânicas
November 22-26, 2021, Virtual Congress, Brazil

COB-2021-1953
DETERMINATION OF INSTALLATION SITES OF HYDROKINETIC TURBINES DOWNSTREAM OF THE SEFAC HYDROELECTRIC FACILITY

Kaajal Gopie
Isadora Montenegro Bugarin
Rafael Castilho Faria Mendes
Taygoara Felamingo de Oliveira
Antonio Cesar Pinho Brasil Junior
University of Brasília, Faculty of Technology, Laboratory of Energy and Environment.
kaajal.gopie@aluno.unb.br; isadorabugarin@gmail.com; rafael.cfmendes@gmail.com; taygoara@unb.br; brasiljr@unb.br

Abstract. *The hydrokinetic potential of electricity generation from a river stretch is studied using numerical methods for turbulent flows. This energy potential will be used to locate areas with high hydrokinetic energy. Areas with a high energy potential make for excellent turbine installation locations. The studied area (SEFAC channel) is located in the São Marcos river, downwind the dam of the SEFAC hydroelectric facility. The geometric data of the natural channel was generated by field experiments using Acoustic Doppler Current Profiler (ACDP) methods. The flow boundary conditions were defined by considering the actual flow rate of the facility. The numerical methodology was verified using experimental data for sinusoidal open channel flow available in the literature. Three different turbulence models are tested for both the methodology validation and the natural channel simulations: the Reynolds Stress Model (RSM), the k-ϵ and the k-ϵ EARSM model. The free surface is simulated considering a slipping boundary. We use the simulations to look for useful sites for hydrokinetic unit installations, considering the local flow velocity, channel depth, secondary currents occurrence, and turbulent kinetic energy levels. A rarely used geometric model and a more accurate siting of turbines, taking also turbulence into consideration, are intended to fill in a knowledge gap in the literature. The proposed methodology has been validated by simulating natural channel flow with accurate results. Out of the three turbulence models, the RSM has provided the most consistent and reliable results. A distinguishing feature of the SEFAC channel, a depression area right after the channel inlet is also presented, with interesting flow structures. Based on high local velocities and depths, a selection of 20 possible turbine locations has been made. Ultimately, the initial proposed 20 locations are narrowed down to seven, using the occurrence of secondary currents and the turbulence intensity as deciding factors.*

Keywords: *hydrokinetic potential, numerical simulation, turbine sites*

1. INTRODUCTION

In a world with depleting fossil fuels reserves and an increased greenhouse effect, the existence of renewable energy resources takes on a significant role in providing energy. These resources are not only sustainable, and as their name itself suggests, renewable, but are also environment friendly. Of all known renewable energy sources, hydropower would be the most efficient and largest resource (S.A., 2015; Barta *et al.*, 2011; Office, 2021; Laws and Epps, 2016). One method to generate energy from water is via hydrokinetic technology (Yuce and Muratoglu, 2015). This type of energy conversion device eliminates the need for the construction of a dam or water reservoirs for hydroelectric facilities, as they need no or little elevation to generate energy (Khan *et al.*, 2009). These systems simply convert the kinetic energy present in flowing water into electric energy (Güney and Kaygusuz, 2010). As the water flowing downstream of hydroelectric facilities often enough still has a kinetic potential, the available energy can be exploited by installing hydrokinetic turbines downstream of the facility.

In order to implement the hydrokinetic technology, the available hydrokinetic energy potential in the waters of where the system is to be used must be studied thoroughly (Liu and Packey, 2014). As in this paper this technology is to be implemented ultimately in a natural channel, the flow behavior of such a channel will be studied. The biggest challenge in estimating the hydrokinetic potential in a natural channel is the difficulty in modeling the flow field (da Silva Holanda *et al.*, 2017). The flow structure of an open-channel flow is complex and varying, as a three-dimensional (3D) interaction between takes place between the fluid, channel walls and bed. This interaction involves especially parameters as gravity, turbulence and roughness. The combination of these factors make the study of open channel flow challenging. However, by using computational fluid dynamics (CFD), this problem can be resolved with a more complete and detailed modeling

of the channel and fluid flow analyzation (Santos *et al.*, 2019; Knight *et al.*, 2005).

Over the years, a rising amount of researches have been dedicated to the study of open-channel flow in artificial channels by numerical simulation (Sahoo *et al.*, 2020; Blanckaert and Graf, 2001; Tang *et al.*, 2015). The artificial channels are specifically constructed to imitate natural flow behavior. The majority of the researches utilize Reynolds Averaged Navier Stokes (RANS) turbulence models to generate results. In the article written by Kamel *et al.* (2014), an attempt is made to develop a numerical method to predict the flow in river bends (curves). The bends have various curvatures and width-depth ratios. Their method uses the 3D non-linear k-ϵ model for a meandering compound channel with a rectangular cross-section. As this turbulence model managed to successfully predict the flow structures and velocity distributions along the channel, makes it possible to be applied for natural channels. This model also managed to demonstrate the presence of an important feature in natural channels: secondary currents. These currents have a noticeable effect on the flow structures and are caused by turbulence anisotropy. Two other works that also managed to demonstrate the presence of secondary currents are that of Jing *et al.* (2009) and Jing *et al.* (2011). Both studies used the Reynolds Stress Model (RSM) to simulate the flows in compound channel meandering flows with different cross sections. The study conducted by Jing *et al.* (2009) simulates the channel with a semi-natural cross section, while the research by Jing *et al.* (2011) apply the RSM to a channel with a trapezoidal cross section. Both studies show a thorough analysis of the secondary flow by varying water depths. Furthermore, the results are in concordance with experimental data, making the RSM one more turbulence model suitable for predicting natural channel flow.

In this case of modeling a natural channel for CFD simulations, information about the velocities, depths, and relief of the river, in other words, the bathymetry of the channel is required. Modeling the channel will allow for determining high velocity areas, resulting in potential locations for the turbines (Holanda *et al.*, 2017). An extensive literary review shows that turbine siting is part of a site or resource assessment study. These studies revolve around several types of current energy: tidal (including straits and estuaries) (Thiébaut and Sentchev, 2016), ocean (Meyer and Van Niekerk, 2016) and river (d'Auteuil *et al.*, 2019) current energy. The general methodology, regardless of the type of current energy, remains unchanged. The majority of the studies start out by simulating the currents using numerical hydrodynamic models, such as Coastal Ocean Marine Prediction Across Scales, (COMPAS) (Marsh *et al.*, 2021) or the Finite Volume Community Ocean Model (FVCOM) (Tang *et al.*, 2014), rendering (mostly) two-dimensional unstructured meshes. The simulated results are calibrated and validated against high frequency radar or bathymetric field data. The next step would be to localize the highest velocities (with high energy potential) in the studied area for siting the turbines. For shallower areas, the depth also becomes a deciding factor (Nguyen *et al.*, 2020). It is thus noted, that in the assessment studies, the aim of turbine siting lies more on extracting the highest amount of energy from a potential site, rather than determining an optimal turbine installation site, as most studies strictly focus only on the velocity and depth and do not consider the negative impact of turbulence on the turbines. The literary review also showed the lack of geometric models based on bathymetric field data. This type of modeling has only been encountered in Santos *et al.* (2019), where the authors carry out a hydrokinetic potential and economic analysis of hydrokinetic turbines implementation in two rivers.

The main contribution of this work to the literature is to fill in the knowledge gaps presented in the previous paragraph. An emphasis is placed on turbine siting by taking an important factor like turbulence and results from multiple turbulence models into consideration. Moreover, present study relies completely on CFD numerical tools, generating an unstructured 3D mesh from bathymetric field data, instead of utilizing a hydrodynamic model. In this research, aforementioned mesh type will be generated to determine possible installation sites for hydrokinetic turbines downstream the dam of the SEFAC hydroelectric facility in the São Marcos river. The entire process of modeling the channel up till determining the turbine sites consists of an extensive numerical investigation, of which the results are presented in this work.

2. NUMERICAL METHODOLOGY

The first step in this numerical investigation process is the validation of the proposed methodology using a benchmark channel. Once the method is validated, the research progresses to numerical simulations with the computational mesh generated using bathymetric data.

2.1 Methodology validation

The benchmark chosen is an artificial meandering channel flow with a trapezoidal cross section (natural channel characteristics), reported by Jing *et al.* (2011). The simulated results are compared to experimental results. The geometry encountered, is model FCF-23B (Fig. 1). This experimental model is installed in the Science and Engineering Council Flood Channel Facility (SERC FCF). This facility has been especially constructed for research in the hydraulic behavior of rivers and flood alleviation channels for when the water flows out of the bank (Knight and Sellin, 2007). The benchmark channel has a trapezoidal cross section with a slope of 45°, also seen in Fig. 1.

The mesh has been generated in ANSYS meshing using tetrahedral elements with a linear global element order of 0.05 m. This element type is chosen to obtain a high quality mesh for the curving complex geometry. For the walls (including the bottom of the channel), the inflation layer option was utilized, with 15 layers and a first layer size of 3.8×10^{-4} m.

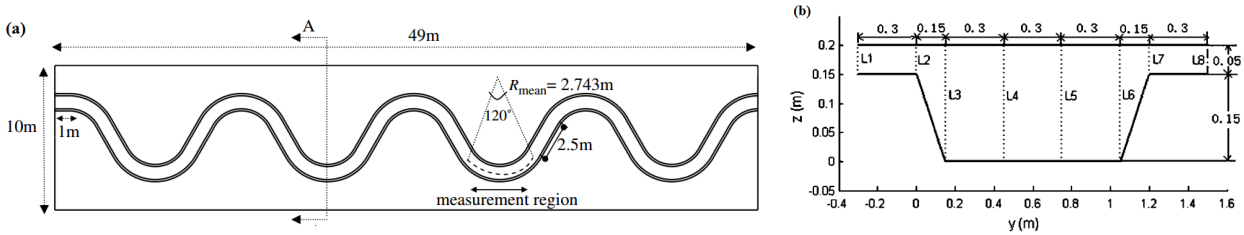

Figure 1. Benchmark channel geometry with a cross over of 60°(a) (Farshi *et al.*, 2018) with the cross section (b) (Jing *et al.*, 2011).

The generated mesh has 3053323 nodes and 6973984 elements with an average y^+ of 7.28. For the simulation, case 3 of Jing *et al.* (2011) has been considered. The details of this case can be found in Tab. 1.

Table 1. Case 3 inlet values by Jing *et al.* (2011).

DR	**Q (m^3/s)**	**H (m)**	**U_{in} (m/s)**	**k_{in} (m^2/s^2)**	**ϵ_{in} (m^2/s^3)**
0.25	0.2480	0.2	0.378	2.14×10^{-3}	8.14×10^{-4}

The kinetic energy turbulence k_{in} and its dissipation rate ϵ_{in}, evaluated by (Choi and Kang, 2008; Guo *et al.*, 2009; Jing *et al.*, 2009), are calculated respectively by Eq. (1) and Eq. (2)

$$k_{in} = \frac{3}{2}(IU_{in})^3, \tag{1}$$

$$\epsilon_{in} = c^{3/4}\mu\frac{k_{in}^{3/2}}{0.1R}, \tag{2}$$

in which I is the turbulence intensity, assumed to be 10% and R is the hydraulic radius. At the inlet, the average velocity U_{in} is determined with $U_{in} = Q/A$, in which Q is the flow rate and A the cross sectional area of the inlet. The relative water depth DR is defined as the ratio between water depth over the flood plain (h) and the maximum water depth in the main channel (H).

At the inlet, a velocity of U_{in} as given in Tab. 1 has been set. At the outlet, the condition of a static pressure equal to zero has been defined, along with a pressure profile blend of 0.05. The walls have a non-slip condition, while the free surface is modeled as a slip wall. The equation class is set to continuity. The simulations are carried out using ANSYS CFX software.

Three additional studies are carried out as part of the methodology validation. In the first one, the mesh is further configured with a convergence study retaining the same boundary conditions and using the k-ϵ model. The mesh is successively refined with an increasing number of nodes. The second study focuses on verifying which turbulence model is able to simulate consistent results closest to the experimental data. Simulations with unchanged boundary conditions with three models (a turbulence model performance study) are carried out: the RSM, the k-ϵ and the k-ϵ EARSM model. Ultimately, the methodology validation itself is realized by comparing results of the most accurate turbulence model from the turbulence model performance study with experimental data by de Lima da Silveira e Lorena (1992).

2.2 Bathymetric data acquisition methodology

The river geometry (bathymetry) is based on depth measurements carried out with a Sontek M9 device, an Acoustic Doppler Current Profiler (ADCP). This tool generates an ultrasonic acoustic wave into the water and detects the backscatter's time from the river bottom and small particles. Following the doppler effect principles, makes it possible to compute the depth and the velocity components over the measured water column. The ADCP was assembled in a boat, as shown in Fig. 2, and was driven along the river. Under this assemble, the data was obtained following the trajectories presented in Fig. 3.

2.3 Numerical simulation using bathymetric data

Using the bathymetry, the computational mesh shown in Fig. 4 has been designed. The geometry has been designed in ANSYS Spaceclaim with an inlet, outlet, a free surface plane and channel walls. The free surface plane is placed at a zero water level.

The mesh has been generated using tetrahedral elements with a linear global element order size of 0.5 m. This element type has been chosen for the same reason as for the benchmark channel: to obtain a high quality mesh for the complex riverbed geometry. The resulting mesh consists of 788902 nodes and 3947129 elements.

Figure 2. Boat (a) with the ADCP assembly (b).

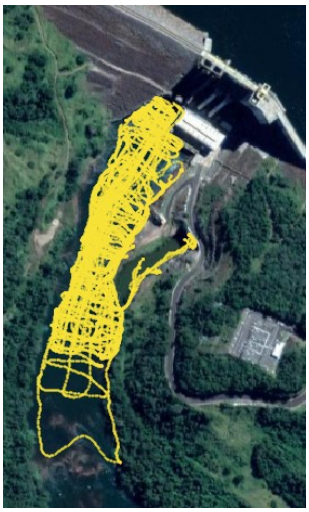

Figure 3. Boat trajectories on the channel taken for the measured depth.

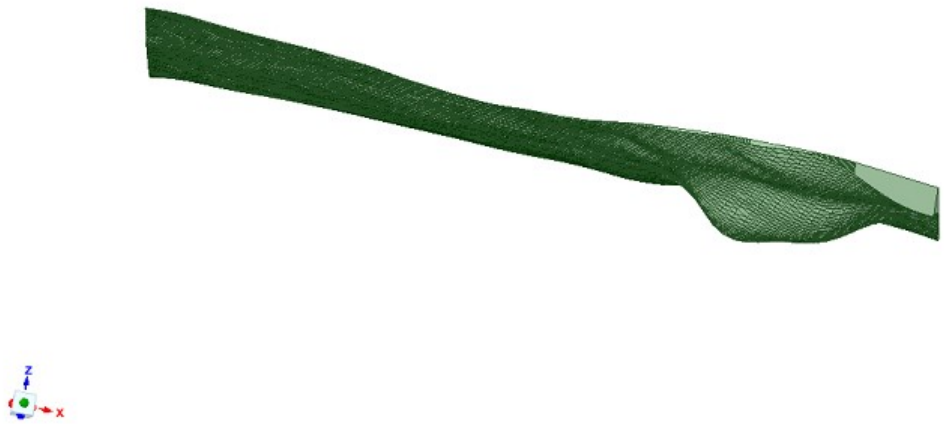

Figure 4. Computational discretized mesh of the SEFAC channel with approximately a length of 345.27 m, maximum depth of 24.50 m and maximum width of 108.99 m.

At the inlet, a flow rate condition of 91 m^3/s has been placed. For the remaining three conditions the same boundary conditions and equation class setting as described for the validation method are considered. The same three turbulence models used in the turbulence model performance study, will be used for the simulations, ultimately basing the turbine locations on the results of multiple turbulence models. These simulations are also carried out using ANSYS CFX software.

3. RESULTS

3.1 Mesh convergence study of the benchmark channel

For the mesh convergence study, the mean velocity U_{mean} has been plotted against an increasing number of nodes. Fig. 5 presents the results of this study. The graph shows the results of four mesh resolutions, with the mesh refined to almost 2.5 million nodes.

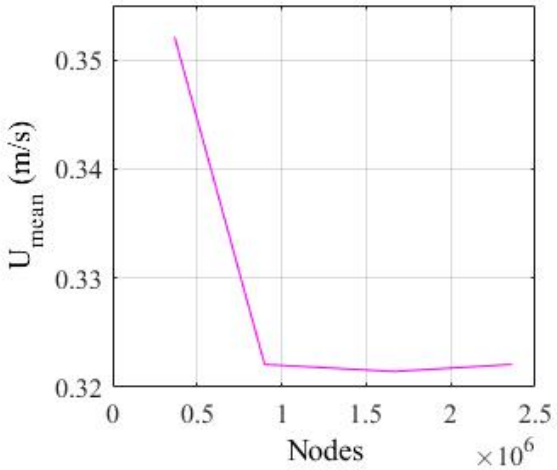

Figure 5. Mesh convergence of the benchmark channel for U_{mean}.

The mean velocity starts out high, decreasing to lower steady values. The graph shows a steady behavior for the last three mesh resolutions, signifying convergence. This convergence proves that the solution of the simulation is independent of the mesh resolution.

3.2 Turbulence model performance study for the benchmark channel

The turbulence model performance study has been conducted for two regions of the cross section presented in Fig. 1: L3 and L5, of which the results are presented in Figures 6 and 7. The axis limits have been adjusted specifically to emphasize the difference in the results of the models. The experimental data has also been plotted only to show whether or not the numerical data shows a similar velocity profile pattern and if so, which model shows the most similar and consistent graph pattern. From there on, the comparison between the best performing model and the experimental data is presented in section 3.3.

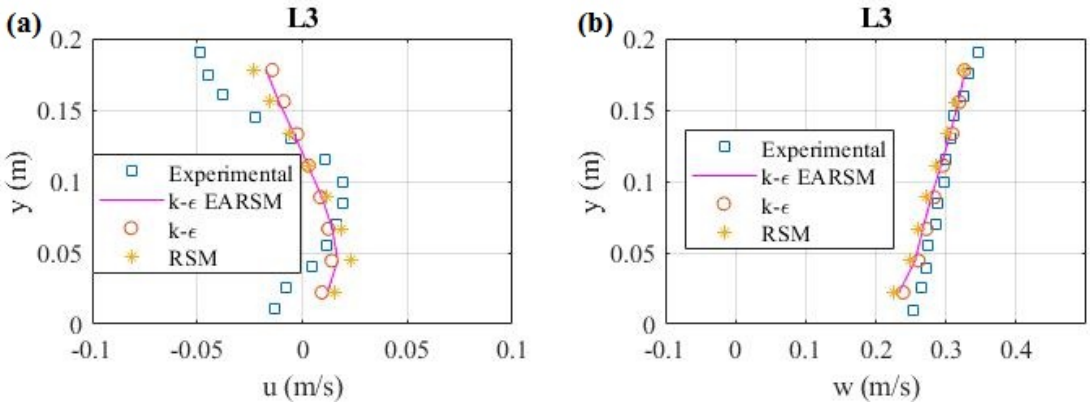

Figure 6. Turbulence model performance comparison plotted with experimental results for transverse velocity u (a) and longitudinal velocity w (b) for L3.

Despite all three models demonstrating a similar velocity profile for all four graphs, the variations in the data can be visualized in three out of four graphs. The only graph where the plotted data of all three models show the highest concordance, is where the numerical velocity profiles differ the most from the experimental profile, which is seen in Fig. 7. Studying the three remaining graphs, shows the RSM displaying the most consistent and similar to experimental velocity profiles, making it suitable to use for the methodology validation.

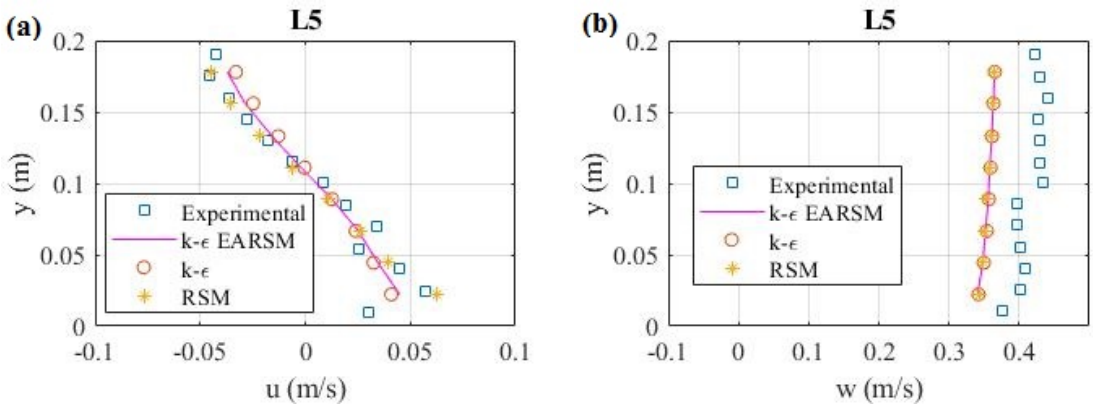

Figure 7. Turbulence model performance comparison plotted with experimental results for transverse velocity u (a) and longitudinal velocity w (b) for L5.

3.3 Methodology validation

Finally, the methodology has been validated by comparing the experimental results with results from the simulation with the RSM. Figures 8 and 9 present the validation results for the transverse and longitudinal velocities for three regions of the main channel. All graphs featured in Fig. 8 show a good concordance between simulated and experimental results. However, in the case of Fig. 9, only one graph shows a good concordance between both results. The discordance between experimental and numerical results is the greatest for the longitudinal velocities, but even so, the velocity profile pattern behavior is maintained by the numerical data. This discordance may have been caused by a complex flow interaction between the floodplain and main channel, as both L4 and L5 are in the middle of the channel cross section and they would be influenced the most by floodplain flow and main channel flow interaction. With the majority of the velocity profiles showing a good agreement between experimental and numerical data, the proposed methodology is deemed capable of reproducing the flow in a meandering compound channel.

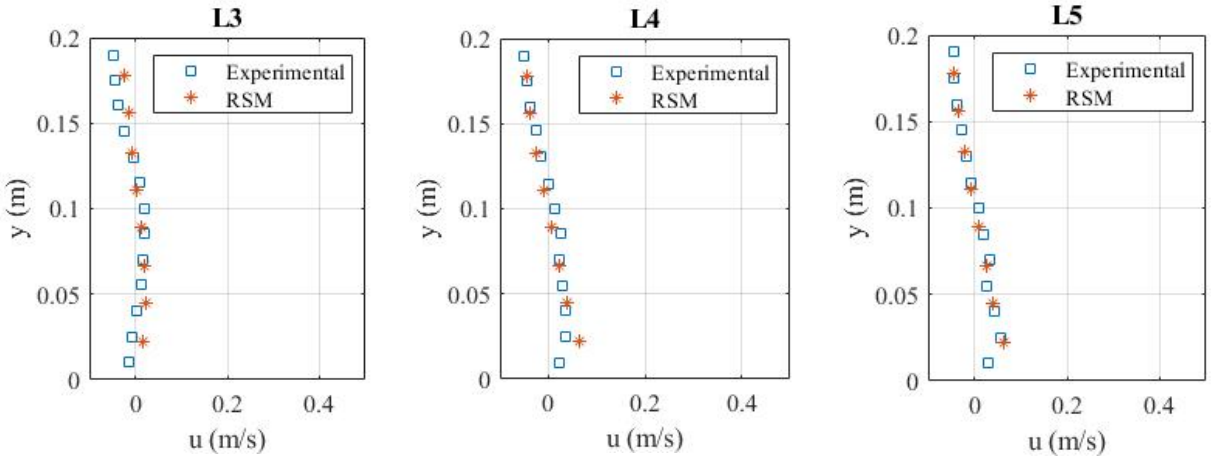

Figure 8. Comparison between experimental and RSM results for transverse velocity u.

3.4 SEFAC channel simulation results

3.4.1 Potential turbine sites

In order to locate potential locations for the turbines, areas of high velocities and large depths must be analyzed. Studying both the velocity and depth contours of the channel, presented in Fig. 10, allows for choosing sections of the channel, where both requirements can be satisfied. The aim is to find areas with a velocity starting from 1 $\mathrm{m/s}$ and a depth of 2 m and higher. Ultimately, five sections seem to fulfill these requirements. In Fig. 10, these five sections, colored with black, made in the channel for further analysis, are presented with section 1 being the closest to the dam. Section 5 appears before section 4, as that section was added later on. The sections in the channel span across the whole channel width and are placed to intersect with the (light) yellow contours. All sections are chosen considering contour maps provided by the three models. Thus, sections 3 and 5 were chosen as a result of respectively the RSM and k-ϵ EARSM model showing a

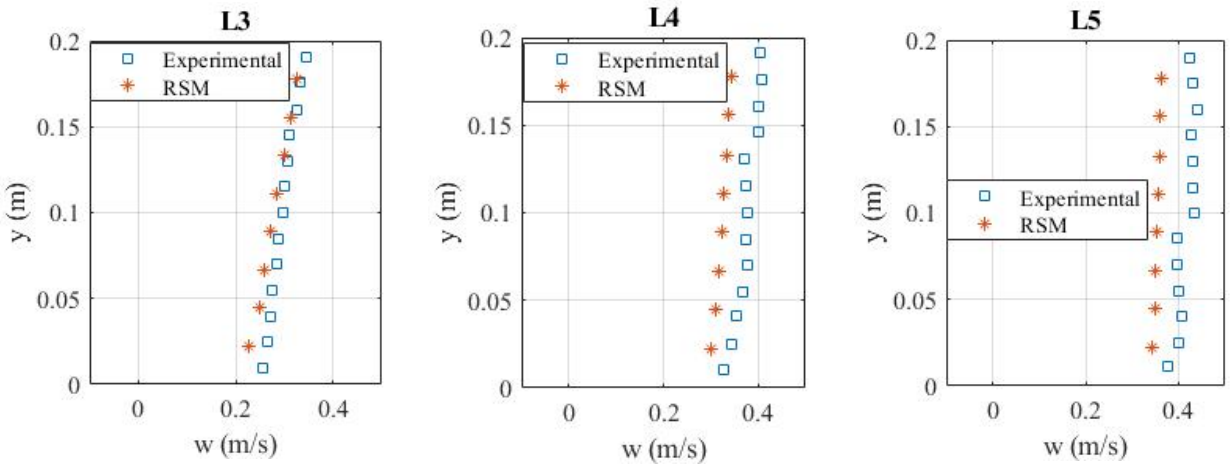

Figure 9. Comparison between experimental and RSM results for longitudinal velocity w.

light yellow-green contour instead of green in Fig. 11. The widest section is section 4, with a width of 103.43 m, while the narrowest is section 1, with a width measuring at 72.58 m. For section 2 a width of 80.28 m is measured, while sections 3 and 5 measure at a width of respectively 88.91 m and 98.04 m.

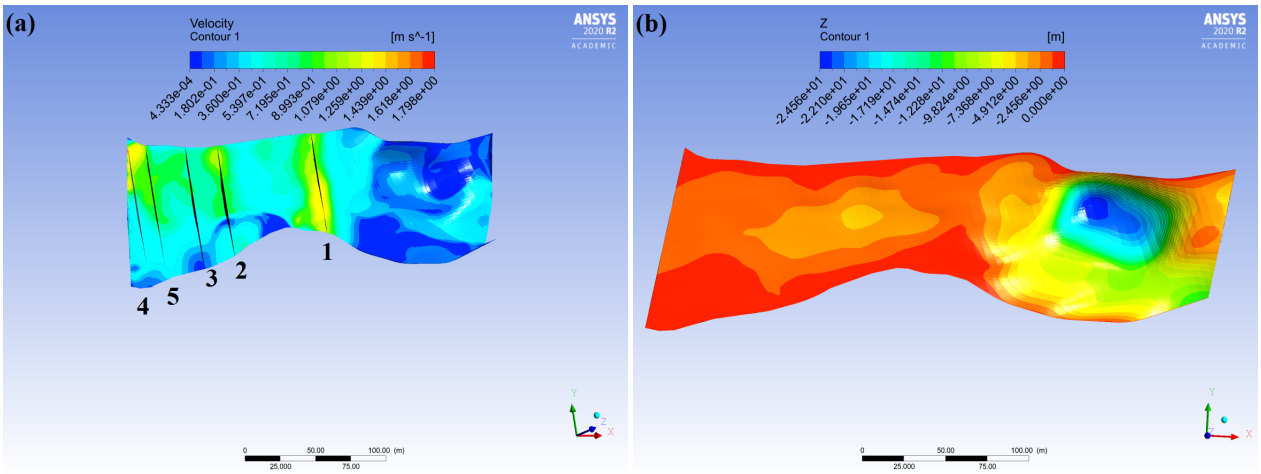

Figure 10. Velocity (a) and depth (b) contours over the SEFAC channel obtained by simulations with the k-ϵ model.

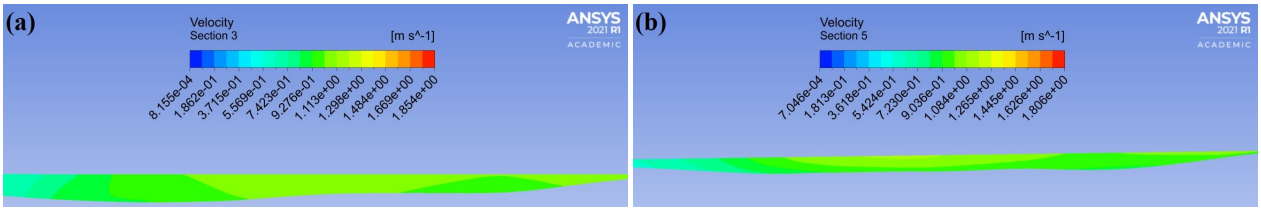

Figure 11. Velocity contours for section 3 (a) by the RSM and section 5 (b) by the k-ϵ EARSM model, focused on the high velocity area.

In each section, four velocity profiles have been chosen (at areas with high velocity and great depth), equally spaced from each other and defined as regions P1 to P4 per section. The potential areas are encountered in the middle of the channel. The search for the installation sites starts with 20 potential locations.

A major consequence of great turbulence is recirculating secondary currents. Finding these currents in one of the sections would help narrow down the number of potential sites. As the currents simulated by the models do not differ, only the currents for the k-ϵ model are presented in Fig. 12 for all five sections, focused on the area of the potential installation sites.

As Fig. 12 presents no recirculating secondary flow occurrence, the potential turbine sites shall have to be analyzed and narrowed down further by studying the turbulence intensity. As all turbulence intensity profiles have the same graph pattern, with the only differences being in depth and intensity value, profiles with a depth close to and higher than 1.5 m

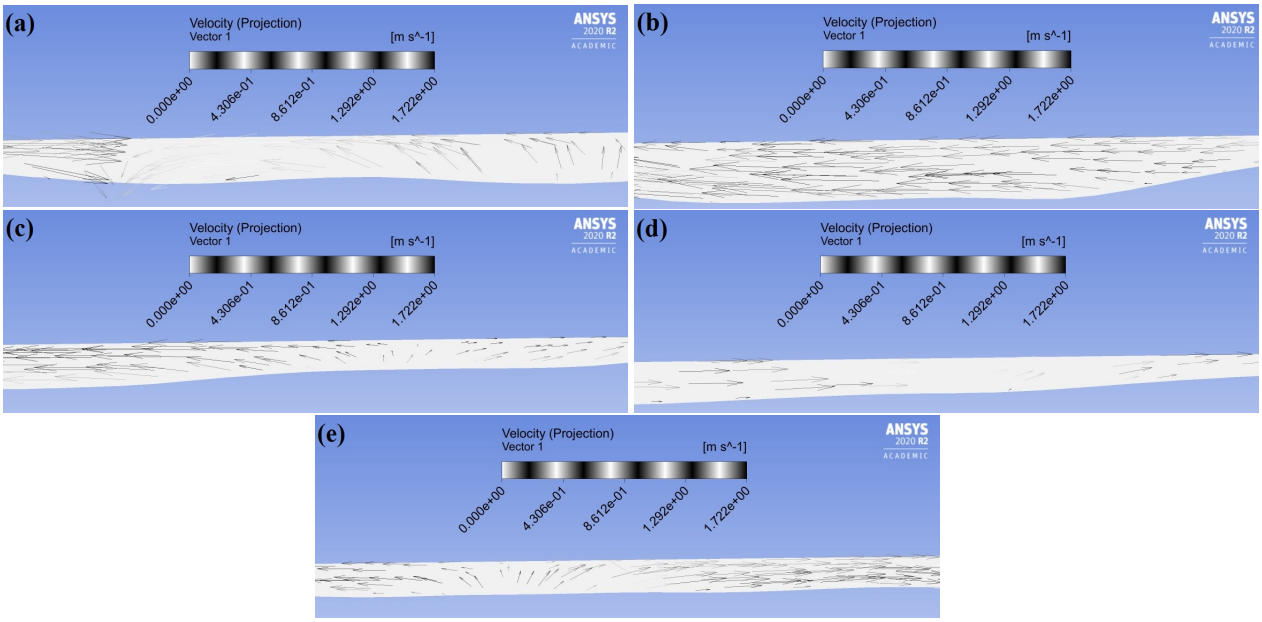

Figure 12. Secondary currents for sections 1 (a), 2 (b), 3 (c), 4 (d) and 5 (e) obtained by simulations with the k-ϵ model.

are shown in Fig. 13.

The maximum turbulence intensity varies from approximately 0.2 to slightly higher than 10 over all profiles. The minimum value is close to zero. The depths vary from approximately 1.4 m to 3 m. The aim was to encounter only sites with a depth of more than 2 m, but sites of 1.4 m depth could also be considered suitable for a small turbine. Noteworthy is the fact that when comparing the results of the turbulence models with each other, the RSM deviates the most in the graphs. The maximum turbulence intensities for the RSM are small, the smallest turbulence intensity not even attaining a value of 0.05. The RSM shows the least dissipation of the turbulent kinetic energy following its graph pattern from riverbed to water level. This fact makes the RSM the most trustworthy model to base turbine siting results on. Even taking the results of the other two models into consideration would not pose difficulties, as the turbines will be located a selected distance above the riverbed, evading the most turbulent areas (near the riverbed), according to Fig. 13. Therefore, all presented profiles in Fig. 13 can be deemed suitable as turbine locations.

3.4.2 Flow in depression area

In Fig. 12 could clearly be seen that no recirculating flow is to be found in any of the sections. This may have to do with the riverbed not being deep enough for recirculating currents. There is however, another area, right after the inlet in the channel, where recirculating flow is certainly to be expected. Unfortunately, this area could not possibly be a potential installation site for the turbines, as the velocity there is the lowest, according to Fig. 10. Despite its unsuitability as an installation site, this depression of 24.5 m in the channel bed does create an interesting situation in the channel flow, featured in Fig. 14.

The transverse velocity is constant over the whole depression area. The flow after the depression area has a lower transverse velocity than is found in the depression itself. This type of depression can be depicted as a type of driven cavity flow. The water flow on the upper surface of the depression creates a shearing force, moving the fluid in the cavity, resulting in a primary vortex and smaller vortices as a result of changes in the wall. In a standard driven cavity flow case, the transverse velocity on the upper surface would be the highest and in the depression the lowest. In the current case, a different result is found, as it is not a standard cavity flow. The depression is not uniformly deep and the fact that it is located right after the inlet may influence the transverse velocity. The main vortex develops in the deepest area of the depression and the smaller vortices in the shallower parts. Despite the differences in transverse velocities between the standard case and the current case, the depression in the SEFAC channel, manages to develop the vortices, which shows a fundamental similarity between both cases.

4. CONCLUSION

In this paper, it is proven that the proposed methodology of simulating natural channel flow is possible and its results are proven to be accurate. The results from simulating the SEFAC channel show five sections along where 20 turbine sites could be located. This channel shows only rotating secondary currents in the depression area, where the lowest velocities of the channel are encountered. Therefore there are no areas of great turbulence narrowing down the potential locations

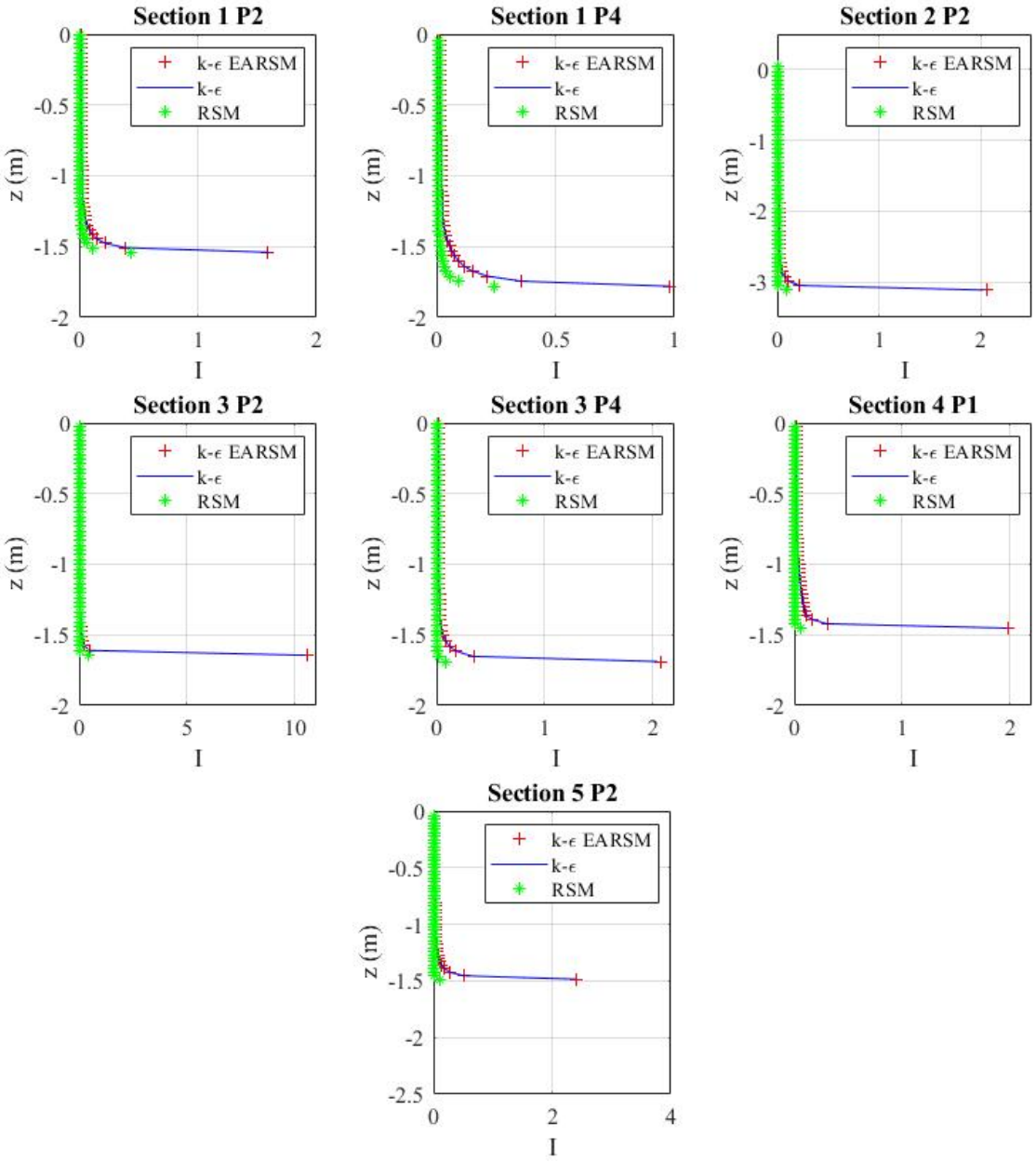

Figure 13. Turbulence intensity profiles of the three turbulence models with highest depth value.

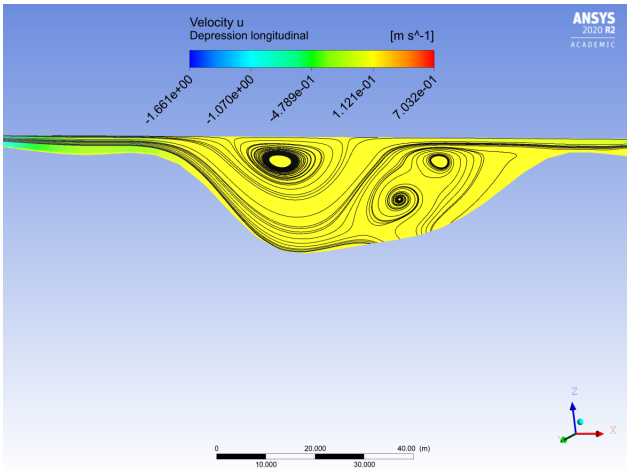

Figure 14. Transverse velocity u contours with streamlines for the cross section in depression area obtained by simulations with the k-ϵ model.

due to rotating secondary currents. In both the methodology validation and the SEFAC channel results, the RSM has provided the most consistent and reliable results out of the three turbulence models. Ultimately, following the analysis of the turbulence intensity per profile carried out in this work, seven locations are deemed suitable as turbine installation sites.

5. ACKNOWLEDGEMENTS

The authors would like to thank Serra do Facão Energia S.A. for providing financial support for the development of the project (ANEEL:P&D06899-2002/2020) - Desenvolvimento de metodologia para determinação de potencial de energia hidrocinética em usinas hidroelétricas.

6. REFERENCES

Barta, B., Van Dijk, M. and Van Vuuren, F., 2011. "Renewable energy: hydropower". *Civil Engineering= Siviele Ingenieurswese*, Vol. 2011, pp. 37–41.

Blanckaert, K. and Graf, W.H., 2001. "Mean flow and turbulence in open-channel bend". *Journal of Hydraulic Engineering*, Vol. 127, pp. 835–847.

Choi, S. and Kang, H., 2008. "Reynolds stress modeling of turbulent open-channel flows". In *Water Resources Research Progress*. Seoul, South Korea.

da Silva Holanda, P., Blanco, C.J.C., Mesquita, A.L.A., Junior, A.C.P.B., de Figueiredo, N.M., Macêdo, E.N. and Secretan, Y., 2017. "Assessment of hydrokinetic energy resources downstream of hydropower plants". *Renewable energy*, Vol. 101, pp. 1203–1214.

de Lima da Silveira e Lorena, M.L.M., 1992. *Meandering Compound Flow*. Ph.D. thesis, University of Glasgow, Glasgow, Scotland.

d'Auteuil, S., Birjandi, A., Bibeau, E., Jordan, S., Soviak, J. and Friesen, D., 2019. "Riverine hydrokinetic resource assessment using low cost winter imagery". *Renewable and Sustainable Energy Reviews*, Vol. 105, pp. 293–300.

Farshi, F., Kabiri-Samani, A., Chamani, M. and Atoof, E., 2018. "Evaluation of the secondary current parameter and depth-averaged velocity in curved compound open channels". *Journal of Hydraulic Engineering*, Vol. 144, p. 04018059.

Güney, M. and Kaygusuz, K., 2010. "Hydrokinetic energy conversion systems: A technology status review". *Renewable and Sustainable Energy Reviews*, Vol. 14, pp. 2996–3004.

Guo, Y., Jing, H. and Li, C., 2009. "Numerical simulation of compound meandering open channel flow". In *33rd IAHR Congress*. Aberdeen, Scotland.

Holanda, P.d.S., Blanco, C.J.C., Mesquita, A.L.A., Brasil Junior, A.C.P., de Figueiredo, N.M., Macêdo, E.N. and Secretan, Y., 2017. "Assessment of hydrokinetic energy resources downstream of hydropower plants". *Renewable Energy*, Vol. 101, pp. 1203–1214.

Jing, H., Guo, Y., Li, C. and Zhang, J., 2009. "Three-dimensional numerical simulation of compound meandering open channel flow by the reynolds stress model". *International Journal for Numerical Methods in Fluids*, Vol. 59, No. 8, pp. 927–943.

Jing, H., Li, C., Guo, Y. and Xu, W., 2011. "Numerical simulation of turbulent flows in trapezoidal meandering compound open channels". *International Journal for Numerical Methods in Fluids*, Vol. 65, No. 9, pp. 1071–1083.

Kamel, B., Ilhem, K., Ali, F. and Abdelbaki, D., 2014. "3d simulation of velocity profile of turbulent flow in open channel with complex geometry". In *8th International Conference on Material Sciences, CSM8-ISM5 2012*. Batna, Algeria.

Khan, M., Bhuyan, G., Iqbal, M. and Quaicoe, J., 2009. "Hydrokinetic energy conversion systems and assessment of horizontal and vertical axis turbines for river and tidal applications: A technology status review". *Applied energy*, Vol. 86, pp. 1823–1835.

Knight, D. and Sellin, R., 2007. "The serc flood channel facility". *Water and Environment Journal*, Vol. 1, pp. 198 – 204.

Knight, D., Wright, N. and Morvan, H., 2005. "Guidelines for applying commercial cfd software to open channel flow". *Report based on research work conducted under EPSRC Grants GR*, Vol. 31, p. 43716.

Laws, N.D. and Epps, B.P., 2016. "Hydrokinetic energy conversion: Technology, research, and outlook". *Renewable and Sustainable Energy Reviews*, Vol. 57, pp. 1245–1259.

Liu, Y. and Packey, D.J., 2014. "Combined-cycle hydropower systems–the potential of applying hydrokinetic turbines in the tailwaters of existing conventional hydropower stations". *Renewable energy*, Vol. 66, pp. 228–231.

Marsh, P., Penesis, I., Nader, J.R., Couzi, C. and Cossu, R., 2021. "Assessment of tidal current resources in clarence strait, australia including turbine extraction effects". *Renewable Energy*, Vol. 179, pp. 150–162.

Meyer, I. and Van Niekerk, J.L., 2016. "Towards a practical resource assessment of the extractable energy in the agulhas ocean current". *International Journal of Marine Energy*, Vol. 16, pp. 116–132.

Nguyen, M.H., Jeong, H., Tran, H.H., Park, J.S. and Yang, C., 2020. "Energy capture evaluation of tidal current turbines arrays in uldolmok strait, south korea". *Ocean Engineering*, Vol. 195, p. 106675.

Office, W.P.T., 2021. "How hydropower works". Office of Energy Efficiency Renewable Energy, How Hydropower Works, https://www.energy.gov/eere/water/how-hydropower-works. Accessed 28 june 2021.

S.A., P.S., 2015. "Fontes de energia renováveis: Tudo o que você precisa saber (in portuguese)". PORTAL SOLAR S.A., https://www.portalsolar.com.br/fontes-de-energia-renovaveis.html. Accessed 18 june 2021.

Sahoo, A., Samantaray, S. and Bikram Singh, R., 2020. "Analysis of velocity profiles in rectangular straight open channel flow". *Pertanika Journal of Science and Technology*, Vol. 28, pp. 1–18.

Santos, I., Camacho, R.G.R., Tiago Filho, G.L., Botan, A.C.B. and Vinent, B.A., 2019. "Energy potential and economic analysis of hydrokinetic turbines implementation in rivers: An approach using numerical predictions (cfd) and experimental data". *Renewable Energy*, Vol. 143, pp. 648–662.

Tang, H.S., Qu, K., Chen, G.Q., Kraatz, S., Aboobaker, N. and Jiang, C.B., 2014. "Potential sites for tidal power generation: A thorough search at coast of new jersey, usa". *Renewable and Sustainable Energy Reviews*, Vol. 39, pp. 412–425.

Tang, L., Sun, H. and Liu, Q., 2015. "Research development of the interaction between turbulence structure and bedforms in open channel". *Advances in Science and Technology of Water Resources*, Vol. 35, pp. 77–84.

Thiébaut, M. and Sentchev, A., 2016. "Tidal stream resource assessment in the dover strait (eastern english channel)". *International Journal of Marine Energy*, Vol. 16, pp. 262–278.

Yuce, M.I. and Muratoglu, A., 2015. "Hydrokinetic energy conversion systems: A technology status review". *Renewable and Sustainable Energy Reviews*, Vol. 43, pp. 72–82.

7. RESPONSIBILITY NOTICE

The following text, properly adapted to the number of authors, must be included in the last section of the paper: The author(s) is (are) solely responsible for the printed material included in this paper.